Journal of Hazardous Materials 166 (2009) 1210–1216

Contents lists available at ScienceDirect

Journal of Hazardous Materials

journal homepage: www.elsevier.com/locate/jhazmat

Nitrogen dioxide formation in the gliding arc discharge-assisted decomposition of volatile organic compounds

Zheng Bo, Jianhua Yan*, Xiaodong Li, Yong Chi, Kefa Cen

State Key Laboratory of Cleaning Energy Utilization, Institute for Thermal Power Engineering, Zhejiang University, Hangzhou, Zhejiang 310027, People's Republic of China

ARTICLE INFO

Article history:
Received 28 July 2008
Received in revised form 3 December 2008
Accepted 4 December 2008
Available online 9 December 2008

Keywords:
Gliding arc discharge
Nitrogen dioxide
Byproduct
Volatile organic compounds
Non-thermal plasma

ABSTRACT

To apply gliding arc discharge (GAD) plasma processing to volatile organic compounds (VOCs) emission control, the formation of NO_2 as an undesired byproduct needs to be addressed. Comparative results of effluent temperature and product concentrations between experiment and thermodynamic equilibrium calculation show that the NO_2 formation in dry air GAD is totally out of thermodynamic equilibrium. Meanwhile, obvious NO ($A^2\sum^+$) and N_2^+ ($B^2\sum_u^+$) are detected as the major reactive species in the dry air GAD plasma region. These results suggest that the thermal (or Zeldovich) NO_x formation mechanism is not significant in GAD system, while the energy level and the density of electrons in the plasma region will severely influence the NO_2 formation. The presence of 500 ppm VOCs in the feed gases shows a limiting influence on the NO_2 formation, which is in the order of aromatic hydrocarbon (C_6H_6 and C_7H_8) > straight-chain hydrocarbon (C_4H_{10} and C_6H_{14}) > halogenated hydrocarbon (CCl_4). The influences of VOCs chemical structure, supply voltage, feed gas humidity, and reactor geometry on NO_2 formation are investigated, and the results correspond to above mechanism analysis. Based on the above, the possible pathways of the inhibition of NO_2 formation in GAD-assisted VOCs decomposition process are discussed.

1. Introduction

The self-oscillating gliding arc discharge (GAD) phenomenon [1–4] produces a plasma region characterized by significant non-thermal property. Most of the energy consumed is used to produce energetic electrons as well as excited ions, atoms and reactive radicals to stimulate the chemical reactions directly and promote selective chemical transition, rather than heat the bulk gas. The potential of GAD has been demonstrated for energy conservation and environmental control, such as gaseous pollutants emission control [5,6], waste water degradation [7,8] and methane reforming [9–11], etc.

Although GAD plasma is clarified as the non-thermal plasma (NTP), it actually presents a dual character of thermal and non-thermal plasma [[1,2,6,7] and references therein]. Compared with other atmospheric electrical discharge NTP systems, the power dispatched in the GAD plasma region is in a relatively high level [7]. As a result, high decomposition rates [12–16] can be achieved when GAD is applied for the decomposition of volatile organic compounds (VOCs), which is a group of gaseous pollutants burdensome for both the environments and human health. The concentrations of VOCs from most of the stationary emission sources are usually in a relatively low level (no more than 10,000 ppm), so the large volume background gas (commonly air) will react intensively with the energetic electrons and reactive species in the plasma region during the VOCs decomposition process. It means that the high energy dispatched in the plasma region is also responsible for the formation of some undesirable byproducts.

The formation of nitrogen dioxide (NO_2) has been considered as a drawback in this technique especially when air is used as the background gas [17]. According to our previous researches [18,19], the concentration of NO_2 in the after discharge effluent could reach a level of several thousands ppm. Kalra et al. have reported that the NO_x generation in GAD strongly depends on the discharge current [20] according to their DC GAD research. However, the particular research on the NO_2 formation in the GAD-assisted VOCs decomposition process has been sparsely documented in the literature.

This study is a continuation of our previous GAD-assisted VOCs decomposition work [18,19,21,22]. NO_2 formation in dry air GAD is mechanistically discussed based on thermodynamic equilibrium calculation and plasma region spectra analysis. Then the influences of VOCs chemical structure, supply voltage, humidity, and reactor geometry on NO_2 formation are experimentally investigated. The pathways of the inhibition of NO_2 formation are discussed based on the above.

* Corresponding author. Tel.: +86 571 87952438; fax: +86 571 87952438.
E-mail address: zjuzhengbo@gmail.com (Z. Bo).

0304-3894/$ – see front matter © 2008 Elsevier B.V. All rights reserved.
doi:10.1016/j.jhazmat.2008.12.030

Nomenclature

B	product
C	NO_2 concentration in the after discharge effluent (ppm)
C(Cal.)	as-calculated NO_2 concentration in the after discharge effluent (ppm)
C(Exp.)	experimental detection of NO_2 concentration in the after discharge effluent (ppm)
C_P(B, t)	thermal capacity respectively for corresponding product B (J/(mol K))
D	smallest distance between electrodes (mm)
DTGs	deuterated triglycine sulfate
FTIR	Fourier transform infrared
GAD	gliding arc discharge
H	vertical distance between electrode throat and nozzle (mm)
I_{RMS}	root mean square value of discharge current (mA)
MCT	mercury cadmium telluride
N(B)	mol number for corresponding product B (mol)
NTP	non-thermal plasma
P	electrical power (kW)
PMT	photo multiplier tube
Q	total gas flow rate (SL/min)
RH	relative humidity (%)
RMS	root mean square
t	outlet effluent temperature (K)
T(Cal.)	as-calculated outlet effluent temperature (K)
T(Exp.)	experimental detection of outlet effluent temperature (K)
U	supply voltage (kV)
VOCs	volatile organic compounds
ΔH_f° (B)	molar formation enthalpy at 298 K for corresponding product B (J/mol)

Greek letter

Φ	nozzle inner diameter (mm)

2. Materials and methods

2.1. Experimental system

A schematic diagram of the experimental system is shown in Fig. 1. The experimental apparatus mainly include a gas supply and regulating line, a 50 Hz GAD reactor with its power supply, and an analysis system.

The feed gases from compressed gas cylinders entered into a 50 Hz GAD reactor after passing through a mixing chamber. The initial VOCs concentration and the feed gas flow rate Q were well adjusted by a set of mass flow controllers. The feed gases could be humidified by a temperature controlled water bubbling system if necessary.

Experiments were conducted at atmospheric pressure and room temperature. The NO_2 concentration in the after discharge effluent C was quantified by means of a NICOLET NEXUS 670 Fourier transform infrared (FTIR) spectroscopy equipped with a DTGs KBr detector. The spectral resolution was set as 4 cm^{-1} and every measurement was repeated four times automatically. The temperature of sample cell was maintained at 180 °C.

The relative humidity of the feed gas was measured using a humidity meter (TES 1360#).

Discharge plasma region spectral analysis was carried out using a grating spectrograph (SBP300). The grating scratch number, blaze wavelength and resolution were set as 1200 g/mm, 350 nm and 0.1 nm, respectively. Spectra data were transferred to a computer with a photo multiplier tube (PMT). The slit width was 50 μm; the step length was set as 0.02 nm and the integration time was 1000 ms.

A DDS69# electronic single phase 2 wires Walt-hour meter (pulse output constant 1600 imp/kWh) was installed in the electric circuit to measure the discharge power P. The discharge voltage and current intensity were measured using a high voltage probe (Tektronix, P6015A) and a current probe (Tektronix, TCP303), respectively, and the signals were sampled through the channels of a digital oscilloscope (Tektronix, TDS2024). 2500 current samples were collected in 50 ms using the Tektronix WaveStar Software v2.4, and the current root mean square (RMS) was calculated as the following equation:

$$I_{RMS} = \sqrt{\frac{1}{2500}\sum_{i=1}^{2500} I_i^2} \quad (1)$$

An electric thermal-couple was used to measure the outlet effluent temperature T(Exp.).

2.2. Plasma reactor

A laboratory scale 50 Hz GAD reactor was used as the plasma source. It mainly consists of two knife-shaped electrodes (96 mm long, 26 mm wide and 4 mm thick) fixed on a Teflon bed plate, a Φ = 1.5 mm in inner diameter gas nozzle, and a quartz encloser. The smallest distance between two electrodes D, and the electrode throat height H (the vertical distance between electrode throat and nozzle outlet) could be well adjusted in the range of 1–4.5 mm and 5–30 mm, respectively. The GAD reactor was supplied with a 50 Hz high voltage transformer (220 V/10 kV) with leakage fluxes. The leakage flux alternately stores and discharges magnetic energy with each electrical cycle and thus effectively acts as an inductor in series in each of the primary and secondary circuits. So the effect of leakage fluxes determines a reactance that produces a constant RMS value of current in the secondary coil, which can protect the transformers well in the gas breakdown. A voltage regular was installed in the electric circuit, which allowed the supply voltage U at different adjustable values (max. U = 10 kV). The detailed descriptions of GAD evolution and supply electric scheme including the leakage flux setup have been presented in our previous articles [11,19].

Fig. 2 presents the plots of discharge voltage and current intensity as a function of time in the relative low gas flow rate condition (5 SL/min). Dry air was used as the feed gas and the supply voltage was set as 10 kV. Both the voltage and current waveforms showed relatively good regularity. The frequencies were appropriately equal to those of the primary voltage, i.e. 50 Hz. In any certain discharge period, the voltage increased to its climax corresponding to a certain initial breakdown, and then reduced sharply in less than 0.02 ms with a current pulse. The maximum value of the quite intense current pulse could reach around 1500 mA, and the peak duration was measured as less than 20 ns.

3. Results and discussion

3.1. NO_2 formation mechanism analysis

3.1.1. Thermodynamic equilibrium calculation

The thermodynamic calculation was carried out to evaluate the thermal (or Zeldovich) NO_x formation in the dry air GAD process. The initial temperature of 20 SL/min feed gases was set as 298 K. Following assumptions were used:

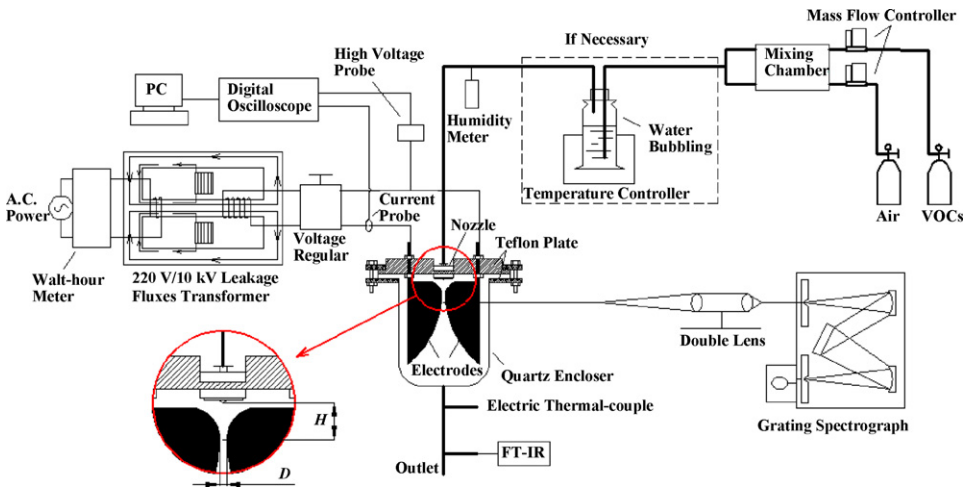

Fig. 1. Schematic diagram of the experiment.

(I) The electrical energy consumption is use to heat the reagents.
(II) The radiation of the reactor can be neglected.

Following the above, the thermodynamic energy balance equation was obtained as

$$P \times 3600 \times 1000 = \sum \left[N(\mathrm{B}) \times \Delta H_f^{\circ}(\mathrm{B})\right] + \sum \int_{298}^{T(\mathrm{Cal.})} N(\mathrm{B}) \times C_P(\mathrm{B}, t)dt \quad (2)$$

where P is the discharge power with the unit of kW, $\Delta H_f^{\circ}(\mathrm{B})$, $N(\mathrm{B})$ and $C_P(\mathrm{B}, t)$ are the molar formation enthalpy at 298 K, the mol number, and the thermal capacity, respectively for corresponding product B.

The dependences of $N(\mathrm{B})$ on the outlet effluent temperature t was obtained using the EQULIB module of FACTsage 5.2 software with the thermodynamical equilibrium reactor model. For 1 mol air (79% N_2 + 21% O_2) reaction, Fig. 3 presents the as-calculated mol number variation of main species (N_2, O_2, NO_2, NO and N_2O) as a function of outlet effluent temperature appearing in entropy maximum condition. Then, T(Cal.) and the as-calculated product concentration C(Cal.) were obtained with Eq. (2).

Table 1 shows the comparative results of effluent temperature and product concentrations between experiment and calculation. Performing above calculation, we could find that the as-calculated effluent temperatures were in the range of 598.2–730.7 K, and the product concentrations were in a relatively low level. It means that the discharge power is not sufficient to support dramatic thermal (or Zeldovich) NO_x formation, which is highly temperature dependent (usually in the temperature > 1800 K), even in the theoretic entropy maximum condition. However, these calculation results could not reflect the true situation, because according to our experimental results the outlet effluent temperatures were significantly lower than the as-calculated values and obvious NO_2 was detected.

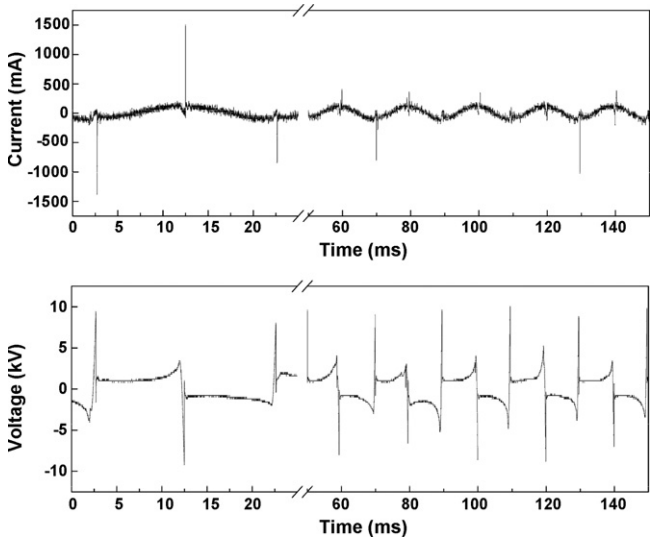

Fig. 2. Discharge voltage and current plots (U = 10 kV; Q = 5 SL/min; Φ = 1.5 mm; D = 3 mm; H = 20 mm; discharge gas: air; RH = 0%).

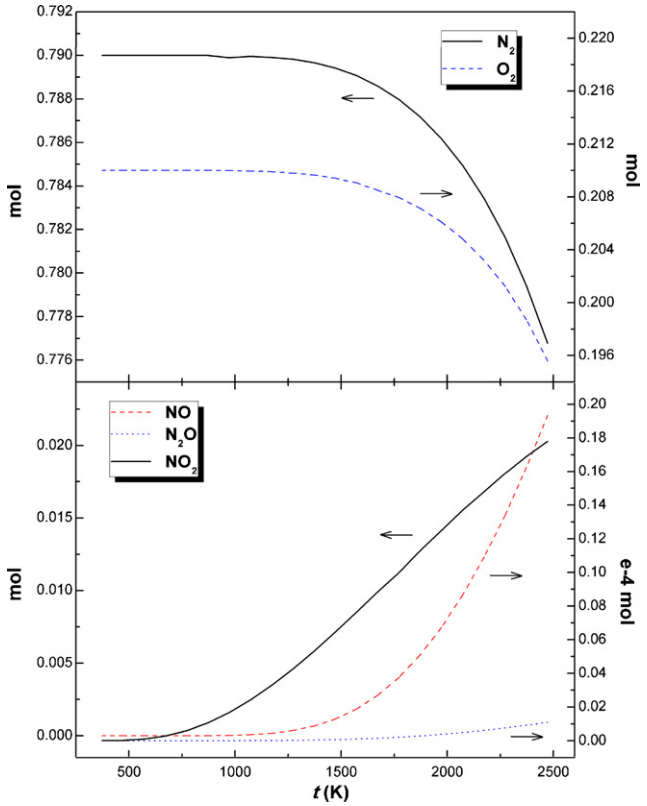

Fig. 3. Thermodynamic equilibrium composition of 1 mol air as a function of temperature.

Table 1
Comparisons of effluent temperature and product concentrations between experiment and calculation.

U (kV)	P (kW)	T(Exp.) (K)	T(Cal.) (K)	C (ppm)			C(Cal.) (ppm)		
				NO	N_2O	NO_2	NO	N_2O	NO_2
7	0.122	309	598.2	–	–	3445.4	5.31e−2	6.07e−6	1.53e−1
8	0.150	317	662.3	–	–	4412.6	4.99e−1	4.77e−5	2.70e−1
9	0.164	326	694.3	–	–	6255.7	2.91	2.42e−4	3.56e−1
10	0.180	333	730.7	–	–	6982.4	12.00	8.92e−4	4.71e−1

It indicates that the thermal combustion process does not play a significant role for the NO_2 formation in GAD system.

3.2. Spectra analysis

In this section, experiments were carried out with dry air as the discharge gas in U = 10 kV condition. The spectroscopic emission detection spot located at 4 cm below the electrode throat vertical along the central axis of the reactor. This point was considered to represent the fully developed GAD region. Fig. 4 shows the emission spectrum in the wavelength scans of 200–400 nm. The spectrum was in a saw-tooth shape, which could be manly attributed to the flashing turbulence discharge. However, several bands could still be identified clearly: NO (transition $A^2\sum^+$, ν = 1 to $X^2\prod$, ν = 0, 237.0 nm; transition $A^2\sum^+$, ν = 2 to $X^2\prod$, ν = 0, 247.9 nm; transition $A^2\sum^+$, ν = 3 to $X^2\prod$, ν = 0, 259.6 nm) in the 200–250 nm scans, N_2^+ (transition $B^2\sum_u^+$, ν = 0 to $X^2\sum_g^+$, ν = 0, 391.4 nm) and N_2 molecule $C^3\prod_u$ to $B^3\prod_g$ transitions between different vibrational levels in the region of 330–390 nm (ν = 0 to ν = 0, 337.1 nm; ν = 0 to ν = 1, 357.5 nm; ν = 1 to ν = 3, 375.5 nm; ν = 0 to ν = 2, 380.5 nm).

The observation of N_2^+ proves the high level of the electrons energy in the GAD plasma region; the normal first ionization potential of nitrogen is as high as 15.58 eV. The detection of NO radicals can be mainly attributed to the recombination of N and O radicals, which indicates that N≡N bonds can be broken into N atoms by the electron impact dissociation in spite of its high bond energy (9.7 eV). NO radical is considered as an important precursor for the generation of NO_2, and the reaction between N radicals and O_2 molecules is another channel of NO_2 formation.

Combining the results in Section 3.1.1, we conclude that the NTP induced reactions dominate the mechanism of NO_2 generation in GAD condition, and consequently, the energy level and the density of electrons in the plasma region will severely influence the NO_2 formation.

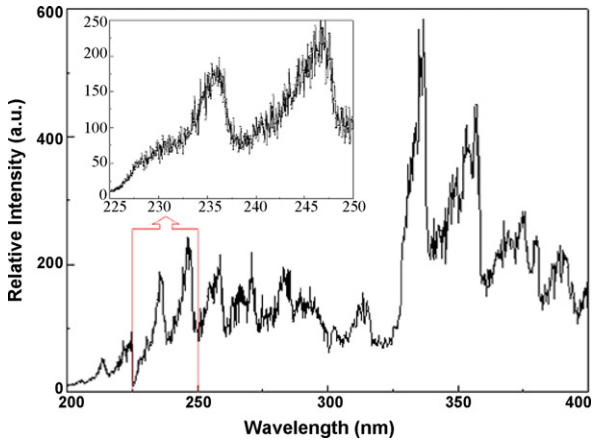

Fig. 4. Spectroscopic emission detected at the spot 4 cm below the electrode throat along the central axis (U = 10 kV; Q = 20 SL/min; Φ = 1.5 mm; D = 3 mm; H = 20 mm; discharge gas: dry air; RH = 0%).

3.3. Effect of VOCs chemical structure on NO_2 formation

Fig. 5 shows the dependence of NO_2 formation on the VOCs chemical structure. Discharges were carried out at the presence of VOCs. Five typical VOCs (i.e. butane (C_4H_{10}), hexane (C_6H_{14}), tetrachloromethane (CCl_4), benzene (C_6H_6), toluene (C_7H_8)) of three types (i.e. straight-chain hydrocarbon, halogenated hydrocarbon and aromatic hydrocarbon) were chosen as the targets. In this section, the water bubbling humidifier was not used.

It was found that the addition of VOCs in the feed gases had a limiting effect on the NO_2 formation. With changing the discharge gas, the NO_2 formation decreased in the order of pure air > air/CCl_4 > air/C_4H_{10} > air/C_6H_{14} > air/C_6H_6 > air/C_7H_8. This observation can be ascribed as followings:

(i) The competition for the electrons and O radicals at the presence of VOCs ((R1)–(R11)), resulting in the inhibition of NO_2 formation.

$$e + CCl_4 \rightarrow CCl_3 + Cl + e \quad (R1)$$

$$n\text{-}C_4H_{10} + e \rightarrow CH_3 + CH_3CH_2CH_2 + e \quad (R2)$$

$$n\text{-}C_4H_{10} + e \rightarrow CH_3CH_2 + CH_3CH_2 + e \quad (R3)$$

$$C_7H_8 + e \rightarrow C_6H_5 + CH_3 + e \quad (R4)$$

$$C_7H_8 + e \rightarrow C_7H_7 + H + e \quad (R5)$$

$$C_7H_8 + e \rightarrow C_5H_6 + C_2H_2 + e \quad (R6)$$

$$C_7H_8 + e \rightarrow C_3H_4 + C_4H_4 + e \quad (R7)$$

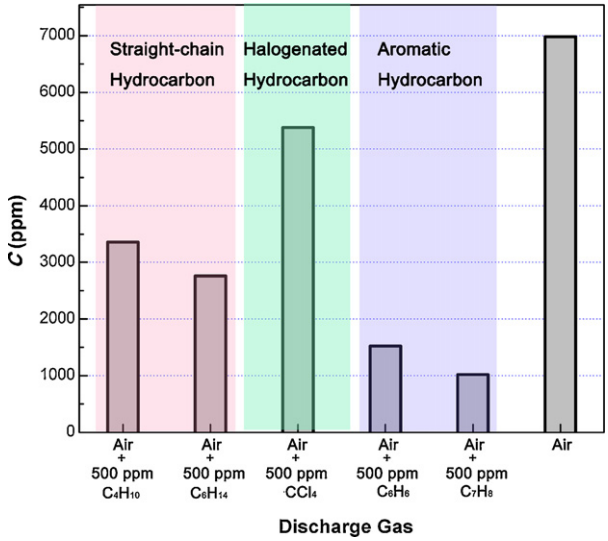

Fig. 5. Effect of VOCs chemical structure on the NO_2 concentration in the after discharge effluent (U = 10 kV; Q = 20 SL/min; Φ = 1.5 mm; D = 3 mm; H = 20 mm; RH = 0%).

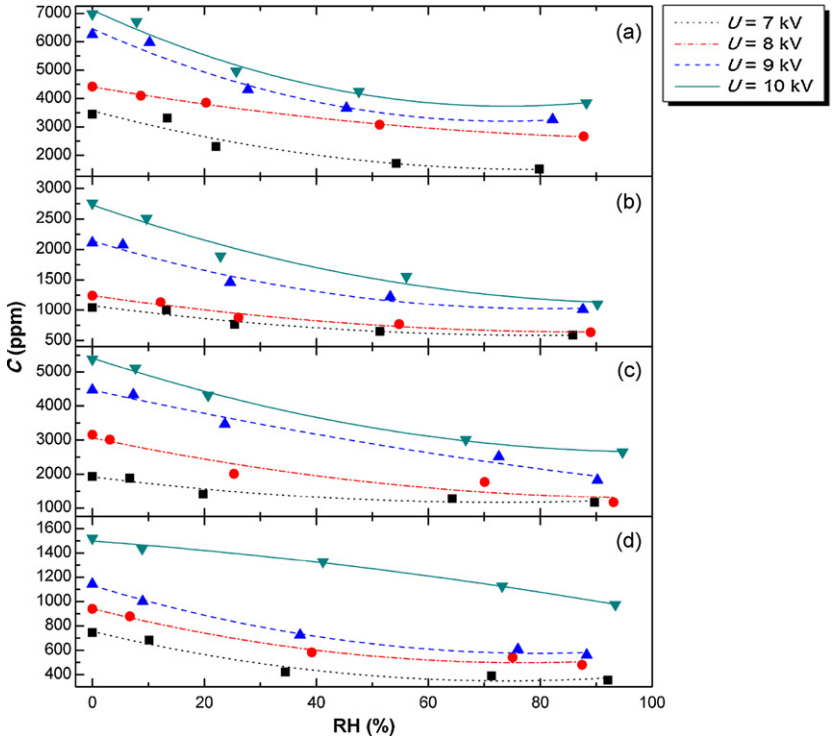

Fig. 6. Effects of supply voltage and background RH value on the NO_2 concentration in the after discharge effluent (Q = 20 SL/min; Φ = 1.5 mm; D = 3 mm; H = 20 mm; discharge gas: (a) air, (b) air + 500 ppm C_6H_{14}, (c) air + 500 ppm CCl_4, (d) air + 500 ppm C_6H_6).

$$O(^1D) + CCl_4 \rightarrow ClO + CCl_3,$$
$$K_{298} = 3.3 \times 10^{-10}\ cm^3\ mol^{-1}\ s^{-1}\ [15] \quad (R8)$$

$$O(^3P) + CCl_4 \rightarrow ClO + CCl_3,$$
$$K_{298} = 3.1 \times 10^{-16}\ cm^3\ mol^{-1}\ s^{-1}\ [15] \quad (R9)$$

$$O + n\text{-}C_4H_{10} \rightarrow n\text{-}C_4H_9 + OH,$$
$$K_{400} = 3.37 \times 10^{-14}\ cm^3\ mol^{-1}\ s^{-1}\ [23] \quad (R10)$$

$$C_7H_8 + O \rightarrow \text{products},$$
$$K_{400} = 3.67 \times 10^{-13}\ cm^3\ mol^{-1}\ s^{-1}\ [24] \quad (R11)$$

(ii) The reactions between NO_2 molecules and OH radicals (formed at the presence of VOCs containing H atoms, *e.g.* (R10)) lead the reduction of NO_2 concentration:

$$NO_2 + OH \rightarrow HO_2 + NO,$$
$$K_{298.15} = 7.7 \times 10^{-16}\ cm^3\ mol^{-1}\ s^{-1}\ [25] \quad (R12)$$
$$NO_2 + OH \rightarrow HNO_3,$$

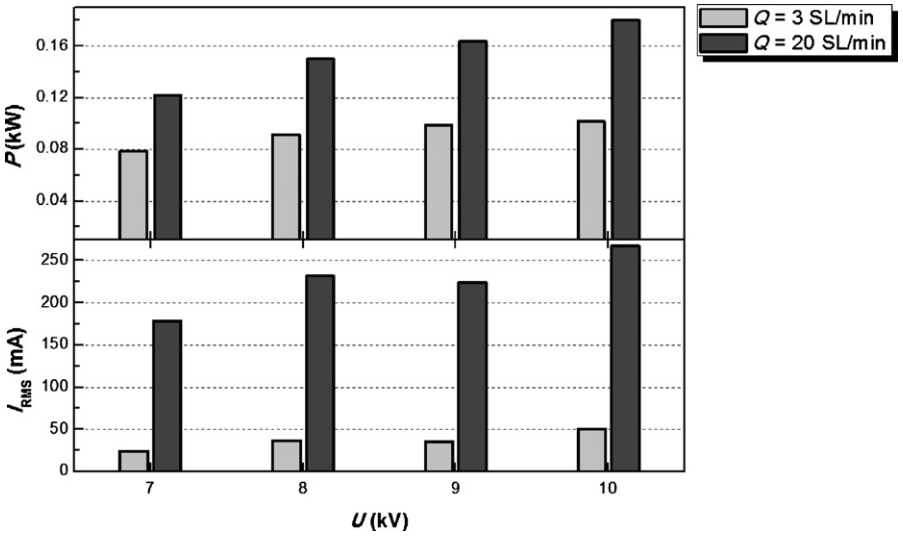

Fig. 7. Effect of supply voltage on the discharge power and current RMS value (Φ = 1.5 mm; D = 3 mm; H = 20 mm; discharge gas: air; RH = 0%).

$K_{298.15} = 2.6 \times 10^{-30}\ cm^3\ mol^{-1}\ s^{-1}$ [26] (R13)

The reactions among OH radicals, C_6H_5 radicals, C_7H_7 radicals and NO_2 molecules provide a possible explanation for the obvious NO_2 inhibition at the presence of benzene or toluene. It is supported by the reported detection of p-aminobenzoic acid [21] and nitrophenol [27] in the after discharge effluent.

3.4. Effects of supply voltage and background humidity on NO_2 formation

Fig. 6 shows the NO_2 concentration in the after discharge effluent as a function of background humidity in different supply voltage conditions. Measurements showed an increasing NO_2 concentration in the after discharge effluent at an increasing supply voltage. This observation was more obvious in the dry air discharges: NO_2 concentration increased from 3445.4 to 6982.4 ppm with the increase of supply voltage from 7 to 10 kV. For any given supply voltage, the addition of water vapor was found unfavorable for the NO_2 formation.

In the dry air discharge conditions, both the energy consumption in the GAD plasma region and discharge current RMS value increased with the increase of supply voltage, as shown in Fig. 7. Similar trends were obtained with using air/VOCs mixture as the discharge gas. The increase of supply voltage led to the increases of both electron energy and density in the plasma region, and consequently more NO_2 was formed and detected in the after discharge effluent.

The inhibition effect of water on the NO_2 formation may be mainly attributed to three possible explanations: due to the large electron attachment coefficient of water molecule, the electron attachment process reduces the number of electrons and quench the energetic electrons; the dissociative attachment of water [26] decreases the electron density; and the enhancement of the reactions between OH radical and NO_2 molecule ((R12) and (R13)).

3.5. Effect of reactor geometrical configuration on NO_2 formation

In a fixed nozzle inner diameter condition (Φ = 1.5 mm), the smallest distance between two electrodes D and the electrode throat height H (the vertical distance between electrode throat and nozzle outlet) are two important parameters of the reactor geometrical configuration. Fig. 8 shows the NO_2 concentration in the after discharge effluent as functions of D and H, with dry air was used as the discharge gas. It was observed that the NO_2 formation increased with the increase of D or the decrease of H.

According to our previous research [22], the maximum length of the arc column increased with the increase of D or the decrease of H, leading to both a larger volume of the plasma region and a higher electrical power sustaining the arc. In current work as seen in Fig. 7, the discharge power P increased from 0.162 to 0.243 kW with an decreasing H from 25 to 10 mm when D = 3 mm, and increased from 0.169 to 0.183 kW with an increasing D from 2.0 to 3.5 mm when H = 20 mm. As a consequence, more energy was dispatched throughout the discharge evolution resulting in more NO_2 was formed.

3.6. Discussion on the pathways of NO_2 formation inhibition

As mentioned above, the increase of supply voltage has a negative influence on the inhibition of NO_2 formation. However, it has been widely recognized that for GAD the increase of supply voltage enhances the decomposition of most VOCs. Combining our previous measurements on the decomposition of butane and toluene with GAD [22], similar conflict between the VOCs decomposition enhancement and the NO_2 formation inhibition also exists

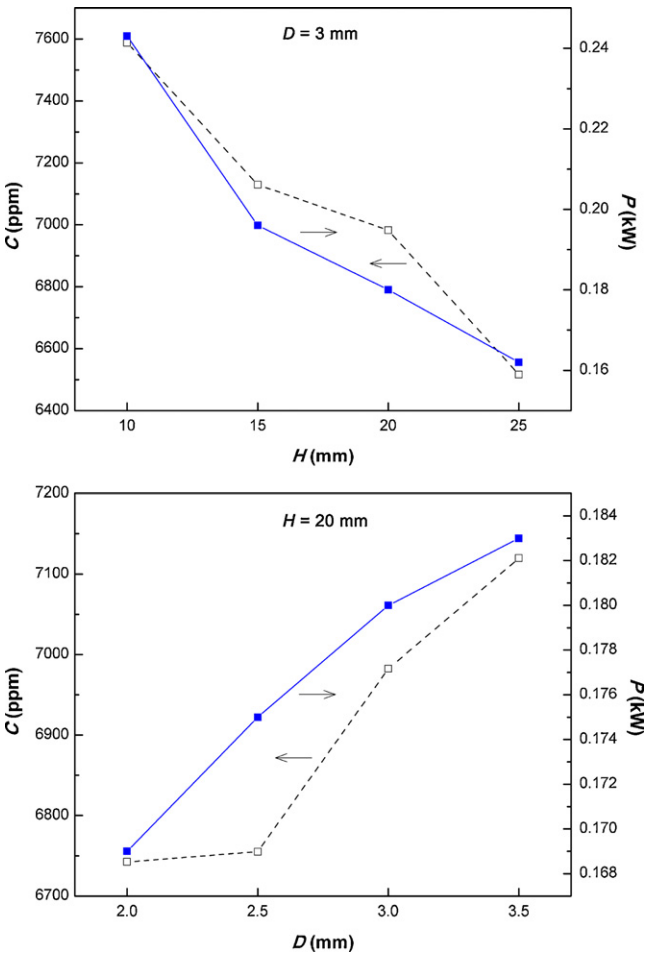

Fig. 8. Effect of reactor geometrical configuration on NO_2 formation and discharge power (Q = 20 SL/min; Φ = 1.5 mm; discharge gas: air; RH = 0%).

in the adjustment of the reactor geometrical configuration: with the increase of D or the decrease of H, the decomposition of VOCs and the formation of NO_2 are enhanced simultaneously owing to a greater electrical power input and a larger probability of the collision between gas (both the VOCs and background gas) molecules and energetic electrons. So, the optimization of reactor structure and power input aiming at promoting the chemical transition selectivity is necessary.

The increase of background humidity has been demonstrated to be favorable for the NTP-assisted decomposition of some VOCs, such as ethanol (C_2H_6O) in microwave plasma reactor [28] and butane (C_4H_{10}) in GAD [21]. In these conditions, the adequate addition of water vapor in the discharge gas would be a proper way for the inhibition of NO_2 formation.

4. Conclusions

NO_2 formation in dry air GAD was totally out of thermodynamic equilibrium, which means the thermal (or Zeldovich) NO_x formation mechanism is not significant in GAD system. With changing the discharge gas, the NO_2 formation decreased in the order of pure air > air/CCl_4 > air/C_4H_{10} > air/C_6H_{14} > air/C_6H_6 > air/C_7H_8, which can be attributed to the competition for the electrons and O radicals at the presence of VOCs, and the reactions between NO_2 and reactive radicals. The energy level and the density of electrons in the plasma region severely influence the NO_2 formation. It is supported by the plasma region spectral analysis and following observations:

the increase of supply voltage increased the NO_2 concentration in the after discharge effluent, while humidity had a limiting effect on the NO_2 formation, irrespective to the feed gas type; the increase of the smallest distance between electrodes or the decrease of the electrode throat height had a positive influence on the NO_2 formation, according to the dry air discharge experiments. In some practical application conditions, the adequate addition of water vapor in the discharge gas would be a proper way for both the enhancement of VOCs decomposition and the inhibition of NO_2 formation. Further optimization is necessary aiming at promoting the chemical transition selectivity.

Acknowledgements

Financial support from National Nature Science Foundation (N50476058) and Science and Technology Bureau of Zhejiang Province is much acknowledged. The support from PRA (Program Sino-French of Advanced Research) was provided by the Institute for Thermal Power Engineering (Zhejiang University, China) and CORIA (France). The programme is authorized by the Ministry of Science and Technology of PRC and the Ministry of Science and Technology of France. The authors gratefully acknowledge the technical assistance for the experimental apparatus afforded by CORIA.

References

[1] A. Fridman, S. Nester, A. Kennedy, A. Saveliev, Gliding arc gas discharge, Progr. Energy Combust. Sci. 25 (1999) 211–231.
[2] O. Mutaf-Yardimci, A.V. Saveliev, A.A. Fridman, L.A. Kennedy, Thermal and non-thermal regimes of gliding arc discharge in air flow, J. Appl. Phys. 4 (2000) 1632–1641.
[3] S. Pellerin, J.M. Cormier, F. Richard, K. Musiol, J. Chapelle, Determination of the electrical parameters of a bi-dimensional D.C. glidarc, J. Phys. D: Appl. Phys. 32 (1999) 891–897.
[4] F. Richard, J.M. Cormier, S. Pellerin, J. Chapelle, Physical study of a gliding arc discharge, J. Appl. Phys. 5 (1996) 2245–2250.
[5] V. Dalaine, J.M. Cormier, S. Pellerin, P. Lefaucheux, H2S destruction in 50 Hz and 25 kHz gliding arc reactors, J. Appl. Phys. 84 (1998) 1215–1221.
[6] A. Indarto, D.R. Yang, C.H. Azhari, W.H.W. Mohtar, J. Choi, H. Lee, H.K. Song, Advanced VOCs decomposition method by gliding arc plasma, Chem. Eng. J. 131 (2007) 337–341.
[7] D. Moussa, J. Brisset, Disposal of spent tributylphosphate by gliding arc plasma, J. Hazard. Mater. B102 (2003) 189–200.
[8] R. Burlica, M.J. Kirkpatrick, B.R. Locke, Formation of reactive species in gliding arc discharges with liquid water, J. Electrostatics 64 (2002) 35–43.
[9] I. Rusu, J.M. Cormier, On a possible mechanism of the methane steam reforming in a gliding arc reactor, Chem. Eng. J. 91 (2003) 23–31.
[10] T. Sreethawong, P. Thakonpatthanakun, S. Chavadej, Partial oxidation of methane with air for synthesis gas production in a multistage gliding arc discharge system, Int. J. Hydrogen Energy 32 (2007) 1067–1079.
[11] Z. Bo, J.H. Yan, X.D. Li, Y. Chi, K.F. Cen, Plasma assisted dry methane reforming using gliding arc gas discharge: effect of feed gases proportion, Int. J. Hydrogen Energy 33 (2008) 5545–5553.
[12] A. Czernichowski, Gliding arc applications to engineering and environment control, Pure Appl. Chem. 66 (1994) 1301–1310.
[13] A. Czernichowski, A. Ranaivosoloarimanana, Zapping VOCs with a discontinuous electric arc, Chemtech 26 (1996) 45–49.
[14] M. Pospisil, I. Viden, M. Simek, S. Pekarek, Application of plasma techniques for exhaust aftertreatment, Int. J. Vehicle Des. 27 (2001) 306–314.
[15] K. Krawczyk, B. Ulejczyk, Decomposition of chloromethanes in gliding discharge, Plasma Chem. Plasma Proc. 23 (2003) 265–281.
[16] K. Krawczyk, B. Ulejczyk, Influence of water vapour on CCl_4 and $CHCl_3$ conversion in gliding discharge, Plasma Chem. Plasma Proc. 24 (2004) 155–167.
[17] K. Urashima, J.S. Chang, Removal of volatile organic compounds from air streams and industrial flue gases by non-thermal plasma technology, IEEE Trans. Dielect. Electr. Insul. 7 (2000) 602–614.
[18] J.H. Yan, Z. Bo, X.D. Li, C.M. Du, K.F. Cen, B.G. Cheron, Study of mechanism for hexane decomposition with gliding arc gas discharge, Plasma Chem. Plasma Proc. 24 (2004) 155–167.
[19] Z. Bo, J.H. Yan, X.D. Li, Y. Chi, K.F. Cen, Scale-up analysis and development of gliding arc discharge facility for volatile organic compounds decomposition, J. Hazard. Mater., doi:10.1016/j.jhazmat.2007.11.105.
[20] C.S. Kalra, A.F. Gustol, A.A. Fridman, Gliding arc discharges as a source of intermediate plasma for methane partial oxidation, IEEE Trans. Plasma Sci. 33 (2005) 32–41.
[21] Z. Bo, J.H. Yan, X.D. Li, C.M. Du, K.F. Cen, B.G. Cheron, Effect of oxygen and water vapor on volatile organic compounds decomposition using gliding arc gas discharge, Plasma Chem. Plasma Proc. 27 (2007) 546–558.
[22] Z. Bo, J.H. Yan, X.D. Li, Y. Chi, K.F. Cen, The dependence of gliding arc gas discharge characteristics on reactor geometrical configuration, Plasma Chem. Plasma Proc. 27 (2007) 691–700.
[23] J.T. Herron, R.E. Huie, Rate constants for the reactions of atomic oxygen with organic compounds in the gas phase, J. Phys. Chem. Ref. Data 2 (1973) 467–518.
[24] R. Atkinson, D.L. Baulch, R.A. Cox, J.N. Crowley, R.F. Hampson Jr., R.G. Hynes, M.E. Jenkin, J.A. Kerr, M.J. Rossi, J. Troe, Summary of evaluated kinetic and photochemical data for atmospheric chemistry (2005, March). Available: <http://www.iupac-kinetic.ch.cam.ac.uk/>.
[25] J. Van Durme, J. Dewulf, W. Sysmans, C. Leys, H. Van Langenhove, Efficient toluene abatement in indoor air by a plasma catalytic hybrid system, Appl. Catal. B: Environ. 74 (2007) 161–169.
[26] Y.S. Mok, I. Nam, Modeling of pulsed corona discharge process for the removal of nitric oxide and sulfur dioxide, Chem. Eng. J. 85 (2002) 87–97.
[27] Z. Ye, Y. Zhang, P. Li, L. Yang, R. Zhang, H. Hou, Feasibility of destruction of gaseous benzene with dielectric barrier discharge, J. Hazard. Mater. 156 (2008) 356–364.
[28] Y.P.I.Y.C. Liu, K.Y. Han, Construction of a low-pressure microwave plasma reactor and its application in the treatment of volatile organic compounds, Environ. Sci. Technol. 38 (2004) 3785–3791.